



Properties of the Passive Film on Alloy 22 in Chloride Solutions Obtained by Electrochemical Impedance

Martín A. Rodríguez^z and Ricardo M. Carranza^z

Comisión Nacional de Energía Atómica, Instituto Sabato, Universidad Nacional de General San Martín, San Martín, Buenos Aires 1650, Argentina

Impedance measurements were performed for alloy 22 in the passive and transpassive range, in 1 M NaCl at 90°C. A R_{Ω} -(R//CPE) circuit model was applied in the full passive range, where R was the film resistance. This model also applied for a wide range of chloride concentrations and pH values, at the open circuit potential. Two time constants were observed at the beginning and at the end of the passive range. In these cases, the resistances for the ion transfer might be located at the film interfaces, and not in the film itself. The protective properties of the film improved with polarization time due to the thickening and ageing of the film. The film resistance and the space charge layer thickness increased with the potential. The oxidation of Cr^{3+} to Cr^{6+} occurred in the film at high potentials, followed by the transpassive dissolution. In the pre-transpassive range of potentials, the film showed a p-type electronic character, while the ionic properties were that of a passive film. The passive film of alloy 22 was an n-type semiconductor, which changed to a p-type for the high passive potentials. $N_D = 2.7 \times 10^{20} \text{ cm}^{-3}$ and $E_{\text{FB}} = -0.551 \text{ V}_{\text{SCE}}$ were determined. © 2011 The Electrochemical Society. [DOI: 10.1149/1.3581034] All rights reserved.

Manuscript submitted September 30, 2010; revised manuscript received February 17, 2011. Published April 21, 2011.

The outstanding corrosion resistance of stainless steels and chromium containing nickel-based alloys is due to the spontaneous development of a chromium-rich passive overlayer. These corrosion resistant alloys require certain minimum chromium content for the passive film to be formed.^{1,2} Passivity results from the formation of a continuous oxide or oxi-hydroxide layer on the metal surface. This thin film protects the alloy against corrosion by isolating it from the corrosive environment.³⁻⁵ Passive films formed on corrosion resistant alloys generally comprise bilayered structures consisting of a defective oxide that grows directly into the metal and an outer hydroxide layer.⁶ Passivity is characterized by a low corrosion rate which is independent of the anodic potential, while the potential is in the passive range.^{3,4} The ionic conduction in passive films is given by point defects such as cation vacancies, oxygen vacancies and cation interstitials. Although the passive films are poor ionic conductors, they may be good electronic conductors.^{5,6} From the standpoint of the electronic properties, the passive films formed on corrosion resistant alloys are semiconductors. They behave as n-type or p-type semiconductors with a very high donor or acceptor concentration. They are also modeled as p-n junctions, with an inner n-type layer and an outer p-type layer, according to their bilayered structure.^{4,6-11}

Alloy 22 (UNS N06022) is a member of the Ni-Cr-Mo family. This alloy offers an outstanding corrosion resistance in a wide variety of highly-corrosive environments.¹ Alloy 22 develops a chromium-rich passive film which is stable even in hot acidic solutions.¹²⁻¹⁸ This alloy is considered for the fabrication of the corrosion-resistant barrier of high-level nuclear waste containers. These containers should fulfill a requirement of thousands years of lifetime.¹⁹ The passivity of alloy 22 has been studied in detail recently, considering that this timeframe of use is beyond any other engineering application.²⁰⁻²⁷

Electrochemical impedance spectroscopy (EIS) and single frequency impedance measurements have been used extensively to study *in situ* the electronic and ionic properties of the passive film developed on alloy 22 and other corrosion resistant alloys.^{14-18,20-27} Impedance data can be analyzed by using an exact mathematical model based on plausible reaction mechanisms that predict the theoretical impedance, such as linearized reaction models; or by empirical electrical analogs (equivalent circuits).²⁸ The point defect model (PDM) is a mechanistic model developed to interpret impedance data from passive systems.²⁹ The passive corrosion of alloy 22, as a potential engineering barrier in high-level nuclear waste isolation, has been successfully modeled in terms of the PDM.²⁰⁻²² The inter-

pretation in terms of equivalent circuits raises some ambiguities, but it is a convenient and simple choice that may provide valuable information. Fitting of electrical analogs to EIS data has been used for obtaining the polarization resistance and the passive film capacitance of alloy 22. The choice of an incorrect equivalent circuit has no consequence for the measured polarization resistance or corrosion rate, since the difference between the limits of the impedance at low and at high frequencies is independent of the form of the reactive components.²⁸ On the other hand, the capacitance values may be more dependent on the proposed equivalent circuit. In the absence of a redox couple in solution, the polarization resistance is related to the ionic properties of the passive film. The interfacial capacitance has been related to the electronic properties of the film.⁶

The definition of an appropriate equivalent circuit for the studied system is the first step in analyzing the impedance data. The R_{Ω} -(R//CPE) equivalent circuit usually fits for most of passive systems.^{14-20,25-27,30} The good fit of simple linear equivalent circuits to the collected EIS data says that the data are reliable, since these circuits fulfill *a priori* the Kramers-Kronig (K-K) transformation. Studies about the K-K transformation of passive alloy 22 are reported elsewhere.^{21,25} The R_{Ω} -(R//CPE) circuit may be reduced to a R_{Ω} -CPE circuit when only the impedance in the high-frequency range is collected. The appearance of additional time constants in the impedance spectra complicates the interpretation of the data in terms of equivalent circuits, since some assumptions should be made. Series and cascade R//CPE equivalent circuits have been proposed for fitting to impedance spectra with more than one time constant.^{14-18,20,30} It is common to associate the time constants with processes within the passive film and at the film interfaces.^{16,20} Other authors have attributed time constants to reactions associated with adsorbed protons at low potentials or with adsorbed anions at high potentials.^{31,32} Most of the authors agrees that the passive film properties are associated with the high-frequency time constant.^{18,20,21,25-27,31}

The results of impedance measurements on passive alloy 22 indicate that the polarization resistance increases with the anodic applied potential in the passive range. This has been attributed to the increase of the passive film thickness.^{21,27} The barrier layer of the passive film is thought to be made of defective Cr_2O_3 ,^{20,22} which is in agreement with the reported composition obtained by *ex situ* microanalysis.^{12,13} The ionic conduction of the film is attributed to interstitial cations (Cr^{3+}) or oxygen vacancies (O^-).^{20,22} The passive film was found to be an n-type semiconductor for low potentials in the passive range, which changes to p-type for higher potentials.^{21-25,27,30} The reported donor concentrations are in the range of 10^{20} - 10^{21} cm^{-3} . The change in the type of semiconductivity is thought to be related with the oxidation of Cr^{3+} to Cr^{6+} in the film and its further dissolution.^{21,22} Nevertheless, the change in

^z E-mail: maalrodr@cnea.gov.ar; carranza@cnea.gov.ar

semiconductivity occurs at potentials significantly lower than that of the current density increase due to the transpassive dissolution.²⁷ Mo and W are reported to be in the outer regions of the passive film. They become important in maintaining low passive currents at high passive potentials.^{12,13}

Important information on the semiconducting properties of passive films has been collected by using the Mott-Schottky (MS) analyses.^{7-11,21-25,27,30} The MS equation establishes a relationship between the space charge capacitance of a semiconductor (C_{SC}) and the applied potential (E) under circumstances where a depletion layer exists at the semiconductor surface.^{28,33} Equation 1 gives the MS relationship for an n-type semiconductor, where E_{FB} is the flat band potential, N_D is the donor density, ϵ is the dielectric constant of the film, ϵ_0 is the vacuum permittivity (8.85×10^{-14} F/cm), e is the electric charge (1.602×10^{-19} C) and k is the Boltzmann constant (1.38×10^{-23} J/K)

$$\frac{1}{C_{SC}^2} = \frac{2}{\epsilon\epsilon_0eN_D} \left(E - E_{FB} - \frac{kT}{e} \right) \quad [1]$$

The study of the semiconducting properties of passive films is obscured by the fact that the measured capacitance is significantly dependent on the selected measurement frequency. The MS analyses are usually performed by impedance data obtained at a single frequency.^{7-11,21-24,27,30} The selection of the frequency for impedance measurements in the MS analyses is not generally based in solid fundamentals. Measurements at high frequencies are preferred since the impedance can be measured quickly and the passive film is slightly modified by the polarization. The selected frequencies range from 1 Hz to 10 kHz. A simple equivalent circuit must be assumed. Most of the authors agree in selecting a series R-C circuit.^{21-25,27,29,31,34,35,42} In some publications, the selected circuit is not explicitly stated.^{9,10,36} Some authors have proposed the parallel R/C circuit for calculating the capacitance of passive films.^{32,37}

The use of a constant phase element (CPE) in electrical analogs to deal with passive alloys as electrodes displaying frequency dispersion is very common in the literature.^{14-18,21,25-27} The frequency dispersion of the passive film properties have been attributed to several sources such as the non-uniform distribution of donors, the contribution of surface states, the dielectric relaxation within the depletion layer, the amorphous nature of the film and the presence of deep donor states.^{28,37} In the recent years, there was a considerable advance in the knowledge of electrodes displaying frequency dispersion obtained by the use of the local EIS (LEIS) technique.³⁸⁻⁴¹ It was determined that geometric current and/or potential distributions by themselves can lead to CPE behavior. A distinction between two-dimensional (2D) and three-dimensional (3D) distributions was stated. In the case of 2D distributions, the origin of the CPE behavior was the distribution of the high-frequency resistance associated with the geometry of the electrode. In the case of 3D distributions, the CPE behavior is due to effects in the normal direction to the electrode surface.³⁸

The problem of the frequency dispersion in the Mott-Schottky (MS) analyses has been recognized and treated in recent publications.^{18,25,42,43} Harrington and Devine developed a procedure which consists in conducting MS tests at different frequencies. Then, the obtained data are used for building a pseudo-EIS diagram for each measured potential.^{25,42} An equivalent circuit including a CPE is used for fitting to the data, and the capacitance is calculated by using an appropriate expression.⁴⁴ Darowicki et al.⁴³ proposed the use of dynamic EIS (DEIS) for determining the MS relationship. DEIS allows obtaining the composition of impedance spectra versus potential. Although the equivalent circuit proposed for fitting does not account for the CPE behavior, the authors indicate that the determination of the space charge capacitance by DEIS does not depend on frequency selection.⁴³

The semiconducting properties of the passive alloy 22 have been studied recently in some detail.^{21-25,27,30} The passive film of alloy 22 is depicted as an n-type semiconductor which changes its charac-

ter to p-type for high anodic potentials. Bellanger and Rameau³⁰ studied alloy 22 in pH 3, Na₂SO₄ at temperatures from 20 to 70°C. The MS analyses led to $N_D = 4.9 \times 10^{20}$ cm⁻³ and $E_{FB} = -0.300$ V_{SCE}. Priyantha et al.²¹ studied the passivity of alloy 22 in pH 3, saturated NaCl at 80°C by electrochemical impedance. They report $N_D = 6.7 \times 10^{20}$ cm⁻³ and $E_{FB} = -0.342$ V_{SCE} obtained from impedance measurements at 5 kHz *via* the MS analyses. Raja et al.^{23,24} performed an MS analyses of passive alloy 22 in 0.5 M H₂SO₄ at 24°C. They measured the impedance at 1 kHz and 3 kHz and reported N_D values from 3×10^{21} to 4.1×10^{21} cm⁻³ and $E_{FB} = -0.248$ V_{SCE}. Harrington and Devine²⁵ report $N_D = 3.3 \times 10^{20}$ cm⁻³ and $E_{FB} = -0.859$ V_{SCE} for alloy 22 in borate buffer solution at 22°C. The high-frequency capacitance data has also been used to calculate the passive film thickness.^{14-17,21,24} This common practice is inconsistent with the observed semiconducting behavior of alloy 22, as pointed out elsewhere.^{18,21} The protective properties of the passive film developed on alloy 22 are attributed to a chromium-rich barrier layer.^{12,13} Comparative studies of the passive films developed in alloy 22 and in pure chromium indicates the passive films only differ in E_{FB} .²⁵ Nevertheless, a controversy exists regarding the semiconducting character of the passive film of chromium. Kong et al.³⁴ reported a passive film of p-type for chromium in sulfate and borate solutions, with pH values ranging from 0 to 10. Kim et al.³⁵ propose an electronic band structure model consisting of an outer p-type Cr(OH)₃ layer and an inner n-type CrOOH layer, with two space charge layers, for chromium in pH 8.5, buffer borate solution. Tsuchiya et al.³⁶ informed that the passive films of chromium and Fe-Cr alloys in 0.1 M H₂SO₄ are composed of an outer Cr(OH)₃ layer (n-type) and an inner Cr₂O₃ layer (p-type) with a p-n heterojunction. Sunseri et al.⁴⁵ suggest that the passive film of chromium in sulfate and borate solutions is an insulator or a slightly p-type semiconductor. Bojinov et al.⁴⁶ indicate that the passive film of chromium in sulfate solutions of pH 0 and 5 is an insulator with an appreciable concentration of defects confined to the interface.

In the present paper, the passive film formed on alloy 22 in chloride solutions at 90°C was studied by electrochemical impedance measurements. The results were analyzed in terms of simple equivalent circuits, as those reported in the recent literature.²⁰⁻²⁷ The aim of the present work was to describe the passive film properties of alloy 22 in terms of equivalent circuit analogs, obtaining information of its ionic and electronic properties.

Experimental

Alloy 22 (N06022) specimens were prepared from wrought mill annealed plate stock. The chemical composition of the alloy in weight percent was 59.56% Ni, 20.38% Cr, 13.82% Mo, 2.64% W, 2.85% Fe, 0.17% V, 0.16% Mn, 0.008% P, 0.0002% S, 0.05% Si, and 0.005% C (Heat 059902LL1). Specimens were used in the mill annealed condition (MA). Two different types of specimens were used (a) Prismatic: a variation of the ASTM G 5 (Ref. 47) specimen, which contains an artificial crevice formed by a PTFE compression gasket; and (b) Cylindrical: a cylinder of 1.9 mm of diameter partially immersed in the test solution without any artificial crevice. The tested surface areas were approximately 10 cm² for the prismatic specimens and 2 cm² for the cylindrical specimens. The specimens had a finished grinding of abrasive paper number 600 and were degreased in acetone and washed in distilled water within the hour prior to testing.

Electrochemical tests were conducted in a one-liter three-electrode vessel (ASTM G 5) (Ref. 47). EIS measurements were performed at the open circuit potential or corrosion potential (E_{CORR}) and also under potentiostatic control. The tests at E_{CORR} were performed in naturally aerated chloride solutions of different concentration and pH. The tests under potentiostatic control were performed in deaerated pH 6, 1 M NaCl. In the latter case, nitrogen (N₂) was purged through the solution 1 h prior to testing and it was continued throughout the entire test. A water-cooled condenser combined with a water trap was used to avoid evaporation of the solution and to

prevent the ingress of air (oxygen). The temperature of the solution was maintained at 90°C by immersing the cell in a water bath, which was kept at a constant temperature. All the tests were performed at ambient pressure. The reference electrode was a saturated calomel electrode (SCE), which has a potential of 0.242 V more positive than the standard hydrogen electrode (SHE). The reference electrode was connected to the solution through a water-cooled Luggin probe. The reference electrode was kept at room temperature. The electrode potentials were not corrected for the thermal liquid junction potential, since it was assumed to be on the order of a few mV.⁴⁸ The counter electrode consisted in a flag of platinum foil (total area 100 cm²) spot-welded to a platinum wire. All the potentials in this paper are reported in the SCE scale. The impedance measurements were carried out using a Solartron SI 1260 impedance/gain-phase analyzer coupled to a Solartron SI 1287 electrochemical interface potentiostat.

The electrochemical tests consisting in three consecutive steps were performed in deaerated pH 6, 1 M NaCl using prismatic and cylindrical specimens. The steps are explained as follows:

- (1) A polarization at an anodic potential until reaching a steady state current.
- (2) An EIS measurement at the corresponding applied potential.
- (3) A single frequency impedance measurement scanning the potential in the cathodic direction.

The potential applied in step 1 was in the range of -0.4 to $+0.4$ V_{SCE}, which covered the passive range and the beginning of the transpassive dissolution. The time needed to reach the steady state (or pseudo steady state) conditions was about 20 h, in most of cases. In step 2, the EIS measurements were performed by superimposing a 10 mV amplitude sinusoidal potential signal to the applied potential. The frequency scan was started at 10 kHz and ended at 1 mHz. An additional EIS test, reversing the frequency scan (from 1 mHz to 10 kHz), was performed in some cases to verify the steady state conditions. Parameters of simple equivalent circuit mathematical models were fitted to these data. The fits were performed with the software ZView 2 version 3.1c, from Scribner Associates, Inc. The errors reported for the fit parameters are those obtained with the software fitting tool. The errors of the calculated parameters were obtained from the propagation of error. The equivalent circuits used in the present paper for fitting to the EIS experimental results are shown in Fig. 1. Step 3 was performed only for the higher applied potentials. A single frequency impedance measurement was performed at a selected frequency, by scanning the potential from the corresponding applied potential to -0.6 V_{SCE}, in steps of 50 mV. Then, the potential scan was reversed, ending at the corresponding initially applied potential. These measurements were used for the MS analyses. The capacitance was calculated according to Eq. 2, by assuming a series R-C equivalent circuit. Z'' is the imaginary part of the impedance and f is the frequency

$$C = \frac{-1}{2\pi f Z''} \quad [2]$$

EIS measurements at E_{CORR} were performed in aerated chloride solutions using prismatic specimens. The equivalent circuit of Fig. 1b was used for fitting to these EIS experimental results.

The equivalent circuits used for fitting to the EIS data included a CPE to deal with the frequency dispersion of the electrode. Brug et al.⁴⁴ and Hsu and Mansfeld⁴⁹ proposed Eqs. 3 and 4, respectively, for calculating the capacitance of an electrode displaying a CPE behavior. C_B and C_{HM} are the capacitances according to Brug et al.⁴⁴ and Hsu-Mansfeld,⁴⁹ respectively; Q and α are the pre-exponential factor and the exponent of the CPE, respectively; R_Ω and R are the ohmic and the polarization resistances, respectively; and f_{HM} is the frequency at which the imaginary part of the impedance shows a maximum

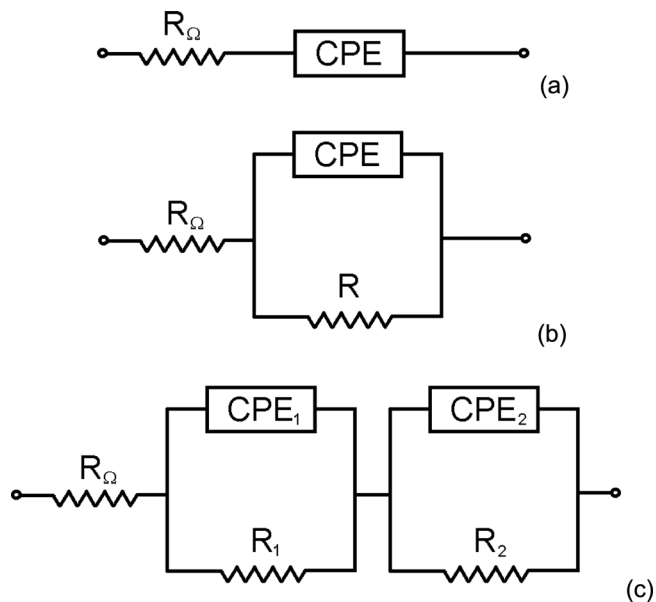


Figure 1. Equivalent circuits used for fitting to the EIS spectra (a) R_Ω -CPE (b) R_Ω -(R//CPE) (c) R_Ω -(R_1 //CPE₁)-(R₂//CPE₂).

$$C_B = Q^{1/\alpha} \left(\frac{1}{R_\Omega} + \frac{1}{R} \right)^{\frac{(\alpha-1)}{\alpha}} \quad [3]$$

$$C_{\text{HM}} = Q(2\pi f_{\text{HM}})^{\alpha-1} \quad [4]$$

For passive alloys in relatively concentrated solutions, $R \gg R_\Omega$ and Eq. 3 can be simplified to Eq. 5. As the studied system is well represented by equivalent circuits of the type R_Ω -(R//CPE), Eq. 4 can be expressed in terms of the fit parameters as Eq. 6.⁴² The calculation of the passive film capacitance from the fit parameters was performed using Eq. 5 (Brug et al.⁴⁴) and Eq. 6 (Hsu-Mansfeld)⁴⁹

$$C_B = Q^{1/\alpha} R_\Omega^{\frac{(1-\alpha)}{\alpha}} \quad [5]$$

$$C_{\text{HM}} = Q^{1/\alpha} R^{\frac{(1-\alpha)}{\alpha}} \quad [6]$$

Results

Figure 2 shows a potentiodynamic polarization curve of alloy 22 in pH 6, 1 M NaCl at 90°C. The range of the performed EIS measurements is shown in Fig. 2. The EIS tests were carried out every 0.1 V, from -0.4 to $+0.4$ V_{SCE}, covering the passive range and the beginning of the transpassive dissolution. Different EIS spectra were obtained depending on the applied potential. The same tests were performed using prismatic and cylindrical specimens. The latter type of specimens was used for avoiding crevice corrosion at the highest applied potentials. The shapes of the EIS spectra were identical for both types of specimens. Additional EIS tests performed reversing the frequency scan led to identical results, indicating that the system was at least in pseudo steady state conditions.

Figure 3 shows the Bode diagram corresponding to an EIS measurement at 0.1 V_{SCE}, in the full passive range. The EIS spectra obtained at potentials from -0.3 to 0.2 V_{SCE} showed a single time constant. Passive alloys are expected to behave as blocking electrodes when tested under potentiostatic control, in the absence of oxidizing species.⁴⁰ This behavior is best represented by a series R_Ω -CPE circuit (Fig. 1a), where R_Ω is the ohmic resistance and the CPE accounts for the frequency dispersion of the passive film properties. Nevertheless, since the low frequency range of the impedance spectra was considered, the R_Ω -(R//CPE) circuit (Fig. 1b) provided

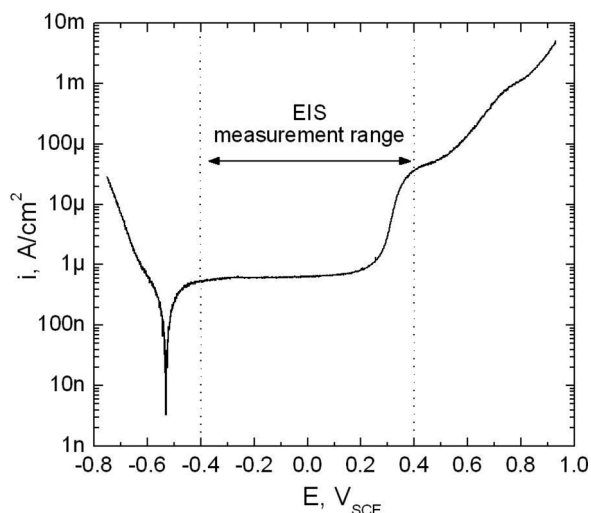


Figure 2. Potentiodynamic polarization curve of alloy 22 in deaerated pH 6, 1 M NaCl at 90°C (scan rate: 0.167 mV/s). The range of potentials for the EIS tests performed under potentiostatic control is shown.

the best fit, and it was used in the present work. The additional resistance of the latter circuit (R) was associated with the passive film resistance, which has a finite value.

Figure 4 shows the Bode diagram corresponding to an EIS measurement performed at $-0.4 V_{SCE}$. A second time constant appeared at $-0.4 V_{SCE}$. The equivalent circuit of Fig. 1c was fitted to the experimental data. The origin of the additional time constant appearing at this low passive potential was not clear. The processes occurring at the metal/passive film interface, at the passive film/solution interface, and within the passive film barrier layer, have been associated to a single time constant each.^{16,20} In the present case, the high-frequency time constant (τ_1) was attributed to processes at the metal/film interface, and the low-frequency time constant (τ_2) was attributed to processes at the film/solution interface. The film barrier layer was assumed to be thin or highly defective at $-0.4 V_{SCE}$, so that the resistances to the ion transfer were located at the film interfaces. Other interpretations of these impedance data were proposed.^{16,20}

Figure 5 shows the Bode diagram corresponding to an EIS measurement at $0.3 V_{SCE}$, in the beginning of the transpassive range.

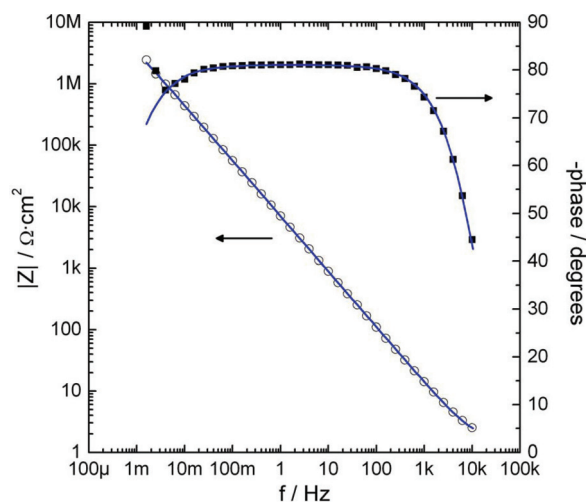


Figure 3. (Color online) Bode diagram corresponding to an EIS measurement at $0.1 V_{SCE}$ for a cylindrical specimen of alloy 22 in deaerated pH 6, 1 M NaCl at 90°C, and the corresponding fit with a R_{Ω} -(R//CPE) circuit (Fig. 1b).

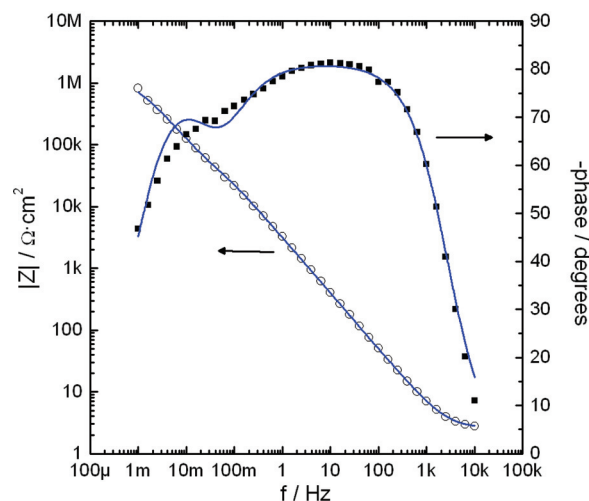


Figure 4. (Color online) Bode diagram corresponding to an EIS measurement at $-0.4 V_{SCE}$ for a prismatic specimen of alloy 22 in deaerated pH 6, 1 M NaCl at 90°C, and the corresponding fit with a R_{Ω} -(R_1 //CPE₁)-(R₂//CPE₂) circuit (Fig. 1c).

The impedance spectra at 0.3 and $0.4 V_{SCE}$ showed two time constants and the equivalent circuit of Fig. 1c was fitted to the experimental data. Again, τ_1 was attributed to processes at the metal/film interface and τ_2 was attributed to processes at the film/solution interface. The barrier layer of the passive film was broken down at these potentials, and a thicker but non-protective transpassive film was developed.¹³ The reaction taking place in the transpassive range was the solid state oxidation of Cr^{3+} to Cr^{6+} within the film, and its further release into the solution.^{21,22,31,46}

Table I summarizes the fitting parameters obtained from all the EIS tests. The polarization at $0.2 V_{SCE}$ and higher potentials using prismatic specimens led to crevice corrosion initiation and these results were discarded. The impedance responses of the two different types of specimens used (prismatic and cylindrical) were similar. The value of α was close to 0.9 for all the measurements in the full passive range (from -0.3 to $0.2 V_{SCE}$), validating the association of the CPE to a frequency disperse electrode. At a potential of $-0.4 V_{SCE}$, the value of α was also close to the unit (0.8–0.93) for the two time constants. At potentials in the transpassive region, the value of α_2 was in the range of 0.8–0.9 (low-frequency time

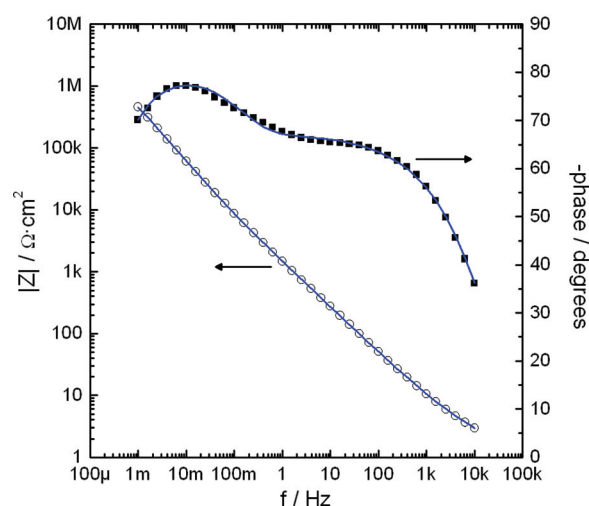


Figure 5. (Color online) Bode diagram corresponding to an EIS measurement at $0.3 V_{SCE}$ for a cylindrical specimen of alloy 22 in deaerated pH 6, 1 M NaCl at 90°C, and the corresponding fit with a R_{Ω} -(R_1 //CPE₁)-(R₂//CPE₂) circuit (Fig. 1c).

Table I. Fit parameters for equivalent circuits corresponding to EIS measurements of alloy 22 in deaerated pH 6, 1M NaCl at 90°C.

E[V _{SCE}]	R _Ω [Ω cm ²]	R or R ₁ [MΩ cm ²]	Q or Q ₁ [Ω ⁻¹ s ²]	α or α ₁	R ₂ [MΩ cm ²]	Q ₂ [Ω ⁻¹ s ²]	α ₂
Cylindrical specimens							
-0.4	1.17 ± 0.04	0.011 ± 0.005	4.1E-4 ± 6E-5	0.80 ± 0.07	1.57 ± 0.05	1.35E-4 ± 2E-6	0.928 ± 0.003
-0.3	1.53 ± 0.04	1.05 ± 0.05	9.33E-5 ± 8E-7	0.879 ± 0.002	—	—	—
-0.2	1.66 ± 0.05	4.9 ± 0.1	7.39E-5 ± 5E-7	0.893 ± 0.001	—	—	—
-0.1	1.73 ± 0.05	8.2 ± 0.4	5.53E-5 ± 3E-7	0.901 ± 0.001	—	—	—
0.0	1.65 ± 0.05	16 ± 2	5.05E-5 ± 3E-7	0.908 ± 0.001	—	—	—
0.1	1.54 ± 0.05	10 ± 2	5.73E-5 ± 4E-7	0.901 ± 0.001	—	—	—
0.2	1.61 ± 0.05	6.2 ± 0.4	7.89E-5 ± 4E-7	0.879 ± 0.001	—	—	—
0.3	1.43 ± 0.02	0.0015 ± 0.0001	9.6E-4 ± 2E-5	0.646 ± 0.002	2.8 ± 0.2	3.93E-4 ± 3E-6	0.886 ± 0.002
0.4	1.32 ± 0.03	0.005 ± 0.001	6.2E-4 ± 3E-5	0.690 ± 0.002	1.7 ± 0.1	2.90E-4 ± 6E-6	0.826 ± 0.005
Prismatic specimens							
-0.4	2.58 ± 0.06	0.0014 ± 0.0005	1.4E-3 ± 2E-4	0.91 ± 0.04	1.2 ± 0.1	8.9E-4 ± 9E-5	0.90 ± 0.02
-0.3	4.03 ± 0.03	2.14 ± 0.05	2.93E-4 ± 1E-6	0.903 ± 0.001	—	—	—
-0.2	3.72 ± 0.06	5.2 ± 0.1	2.58E-4 ± 1E-6	0.910 ± 0.001	—	—	—
-0.1	3.72 ± 0.09	10.5 ± 0.9	2.86E-4 ± 2E-6	0.905 ± 0.001	—	—	—
0.0	2.80 ± 0.04	10 ± 2	2.19E-4 ± 1E-6	0.916 ± 0.001	—	—	—
0.1	3.80 ± 0.09	14 ± 2	2.10E-4 ± 2E-6	0.914 ± 0.001	—	—	—

constant), but α_1 was in the range of 0.65–0.7 (high-frequency time constant). The latter might not be associated with a frequency disperse electrode. At the potentials where two time constants appeared, the high-frequency resistance (R_1) was negligible compared to the low-frequency resistance (R_2) (Table I). In the previous interpretation of the impedance results, the processes at the metal/film interface (τ_1) were faster than those at the film/solution interface (τ_2).

Figure 6 shows the capacitance values calculated according to Brug et al.⁴⁴ (Eq. 5) and to Hsu-Mansfeld⁴⁹ (Eq. 6) as a function of the applied potential, for alloy 22 in 1 M NaCl, at 90°C. Only the measurements in the full passive range (from -0.3 to 0.2 V_{SCE}) were considered. The average value usually assumed for the capacitance of the Helmholtz layer (C_H) is indicated for comparison. The capacitances obtained for cylindrical and prismatic specimens were similar. The values of C_B were consistent with those corresponding to a capacitance of a thin passive film,¹⁸ while those of C_{HM} were significantly higher. The Hsu-Mansfeld⁴⁹ expression led to capacitances higher than those expected for the Helmholtz layer (Fig. 6), which was incompatible with the presence of a passive film.

The values of C_B obtained from Eq. 5 were considered as the series combination of the space charge capacitance of the passive film

and the Helmholtz layer capacitance. C_{SC} was calculated according to Eq. 7, assuming $C_H = 30 \mu\text{F}/\text{cm}^2$

$$C_{SC} = \left(\frac{1}{C_B} - \frac{1}{C_H} \right)^{-1} \quad [7]$$

The values of C_B at -0.4 V_{SCE} (two time constants, τ_1 and τ_2) were $C_{B1} = 39 \mu\text{F}/\text{cm}^2$ and $C_{B2} = 69 \mu\text{F}/\text{cm}^2$, for the prismatic specimens, and $C_{B1} = 24 \mu\text{F}/\text{cm}^2$ and $C_{B2} = 31 \mu\text{F}/\text{cm}^2$, for the cylindrical specimens. In the transpassive range, the values of C_B were $C_{B1} = 8.3 \mu\text{F}/\text{cm}^2$ and $C_{B2} = 65 \mu\text{F}/\text{cm}^2$ at 0.3 V_{SCE}, and $C_{B1} = 8.7 \mu\text{F}/\text{cm}^2$ and $C_{B2} = 23 \mu\text{F}/\text{cm}^2$ at 0.4 V_{SCE}. The capacitance at the metal/film interface (C_{B1}) was the lowest one, both at -0.4 V_{SCE} and at the transpassive potentials. The accumulation of charge at the film/solution (2) interface was larger than at the metal/film (1) interface, which might be related to the higher resistance to the ion transfer ($R_2 \gg R_1$) of the former interface (Table I).

The high-frequency capacitance data are frequently used to calculate the passive film thickness.^{14–18,21,24} In the present case, a semiconducting film was considered, so the thickness obtained with these calculations would be that of its space charge layer. Equation 8, for a parallel plate capacitor, was used for calculating the space charge layer thickness (d_{SC}) in the full passive range. A value of $\epsilon = 30$ was considered based on the literature.²⁰ C_{SC} was obtained from Eq. 7

$$d_{SC} = \frac{\epsilon_0 \epsilon}{C_{SC}} \quad [8]$$

Figure 7 shows the space charge layer thickness and the total resistance to the ion transfer (R or $R_1 + R_2$) as a function of the applied potential. A linear increase of d_{SC} was observed as the potential increased. The error associated with d_{SC} was large since the parameter ϵ had to be assumed and its error was considered to be $\Delta\epsilon = 5$. An anodizing constant of 2.1 to 2.2 nm/V was obtained by least squares fit between -0.3 and 0.1 V_{SCE}, which is in agreement with that reported by Priyantha et al.²¹ The resistance increased with the applied potential from -0.4 to 0 V_{SCE} or 0.1 V_{SCE}, and then it started to decrease. The space charge layer thickness also decreased from 0.1 to 0.2 V_{SCE}. This drop of d_{SC} and the resistance was attributed to the onset of the transpassive reaction.

Experiments were also performed for assessing the effect of the polarization time on the passive film properties, in the full passive range. Figure 8 shows the evolution of R and C_{SC} as a function of the polarization time, at 0.1 V_{SCE}. As the polarization time increased the ionic properties of the film improved (R increased) and C_{SC}

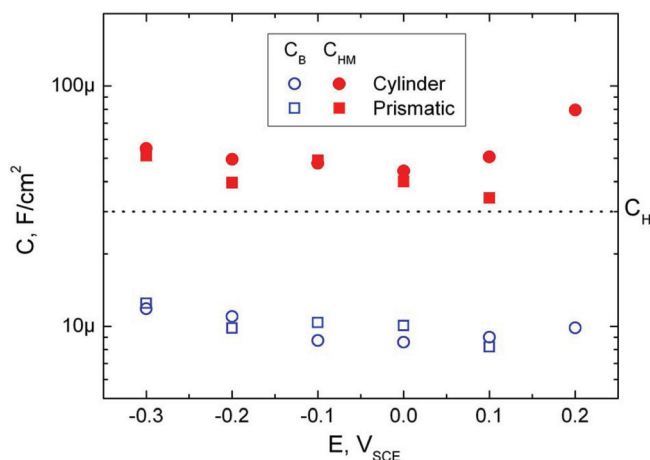


Figure 6. (Color online) Capacitances according to Brug et al.⁴⁴ (C_B) and Hsu-Mansfeld⁴⁹ (C_{HM}) obtained from EIS tests in prismatic and cylindrical specimens of alloy 22, in deaerated pH 6, 1 M NaCl at 90°C.

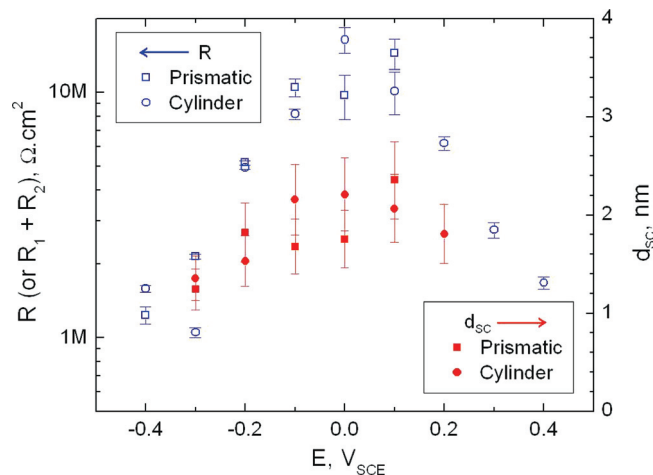


Figure 7. (Color online) Total resistance for ion transfer (R or $R_1 + R_2$) and space charge layer thickness (d_{sc}) as a function of the applied potential for alloy 22 in deaerated pH 6, 1 M NaCl at 90°C.

decreased. These observations suggest a film thickening and possibly the changing of its dielectric properties (ϵ) as the polarization time increased.

Figures 9 and 10 show the Bode diagrams corresponding to EIS tests at E_{CORR} in aerated pH 6, 5 M CaCl₂ and aerated pH 0.4, 0.4 M HCl + 0.6 M NaCl, at 90°C, respectively. The latter solution corresponds to a pH value slightly higher than the depassivation pH in aerated conditions.¹⁸ Several tests were performed after 24 h of immersion in aerated chloride solutions at 90°C, in open circuit conditions. The fitting parameters for a R_{Ω} -(R//CPE) circuit (Fig. 1b) corresponding to these EIS measurements are listed in Table II. In these environmental conditions, the passive dissolution of the alloy was balanced by the reduction of the oxygen dissolved in solution. The same EIS response was observed in a wide range of pH values (from pH 0.4 to 13) and chloride concentrations (0.1 to 10 M). Again, the capacitance values obtained from the expression of Brug et al.⁴⁴ (Eq. 5) were consistent with the presence of a protective passive film. The expression of Hsu-Mansfeld⁴⁹ (Eq. 6) led to capacitance values too large to be compatible with those of a passive film, as reported elsewhere.¹⁸

MS analyses were performed for obtaining information about the semiconducting properties of the passive film. Measurement of the entire impedance spectra at each potential value was not possible

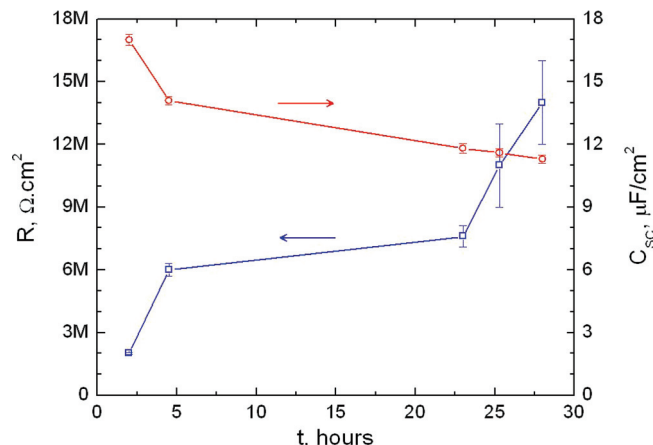


Figure 8. (Color online) Passive film resistance (R) and space charge layer capacitance (C_{sc}) as a function of the polarization time for a prismatic specimen of alloy 22 polarized at 0.1 V_{SCE} in deaerated pH 6, 1 M NaCl at 90°C.

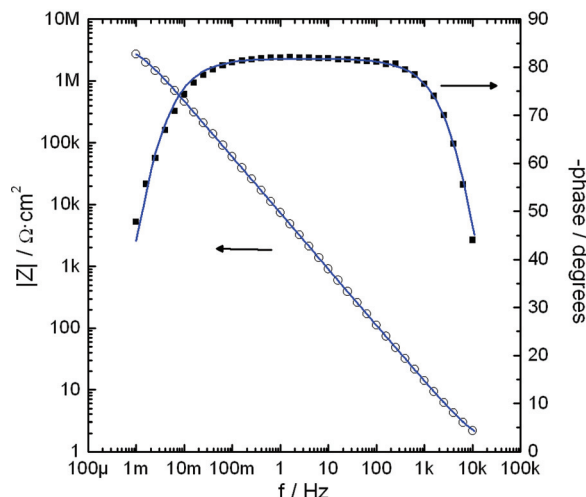


Figure 9. (Color online) Bode diagram corresponding to an EIS measurement after 24 h of immersion at E_{CORR} for a prismatic specimen of alloy 22 in deaerated pH 6, 5 M CaCl₂ at 90°C, and the corresponding fit with a R_{Ω} -(R//CPE) circuit (Fig. 1b).

since the long polarization may cause significant modifications of the passive film properties. The capacitance was calculated from single frequency impedance measurements by assuming a series R-C circuit. In the present work, the passive film of alloy 22 was described in terms of a R_{Ω} -(R//CPE) circuit, in the full passive range. The capacitance C_B was found to be representative of the interfacial capacitance. The correct frequency for obtaining C_B from a single impedance measurement, assuming a R-C circuit, is f_B as defined in Eq. 9 (Appendix)

$$f_B = \frac{1}{2\pi R_{\Omega} C_B} \tag{9}$$

The value of f_B from Eq. 9 depends on the values of R_{Ω} and C_B to be measured. It was assumed that R_{Ω} and C_B in the MS analyses would be similar to that previously obtained from the EIS tests. Considering the data from Table I and Fig. 6, average values of $f_B = 5$ kHz and $f_B = 10$ kHz were calculated for the prismatic and cylindrical specimens, respectively. The MS analyses were

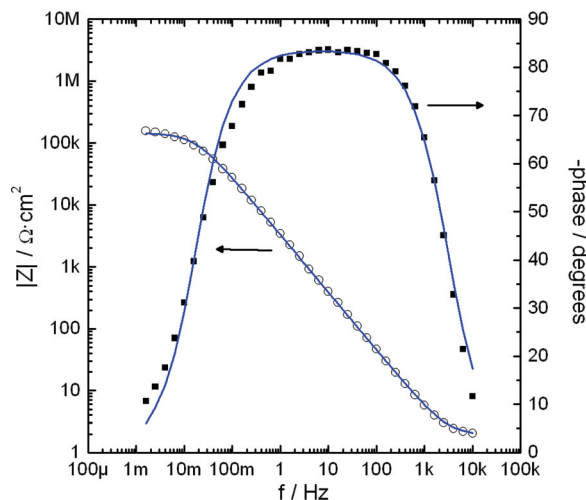


Figure 10. (Color online) Bode diagram corresponding to an EIS measurement after 24 h of immersion at E_{CORR} for a prismatic specimen of alloy 22 in deaerated pH 0.4, 0.4 M HCl + 0.6 M NaCl at 90°C, and the fit with a R_{Ω} -(R//CPE) circuit (Fig. 1b).

Table II. Fit parameters for a R_{Ω} -(R //CPE) circuit corresponding to EIS measurements in prismatic specimens of alloy 22 at E_{CORR} , after 24 h of immersion in chloride solutions at 90°C. C_B and C_{HM} are the capacitances calculated according to Eqs. 5 and 6, respectively.

Solution	E_{CORR} [V _{SCE}]	R_{Ω} [Ω cm ²]	R [M Ω cm ²]	Q [Ω^{-1} s ²]	α	C_B [μ F/cm ²]	C_{HM} [μ F/cm ²]
pH 6, 5M CaCl ₂	-0.140	1.31 ± 0.04	4.4 ± 0.1	2.75E-4 ± 2E-6	0.909 ± 0.001	9.2 ± 0.1	41.2 ± 0.4
0.4 M HCl + 0.6 M NaCl	0.191	1.92 ± 0.05	0.146 ± 0.003	5.74E-4 ± 8E-6	0.930 ± 0.003	27.5 ± 0.5	64 ± 1
pH 1, 1 M NaCl	0.229	3.78 ± 0.06	0.235 ± 0.004	3.99E-4 ± 3E-6	0.940 ± 0.002	23.3 ± 0.2	47.1 ± 0.4
pH 2, 1 M NaCl	0.230	3.75 ± 0.06	2.51 ± 0.06	1.65E-4 ± 3E-6	0.933 ± 0.001	8.0 ± 0.2	21.0 ± 0.5
pH 3, 1 M NaCl	0.036	2.98 ± 0.06	2.28 ± 0.07	3.90E-4 ± 2E-6	0.904 ± 0.001	15.5 ± 0.1	65.5 ± 0.6
pH 4, 1 M NaCl	0.025	3.13 ± 0.03	2.85 ± 0.04	3.64E-4 ± 1E-6	0.917 ± 0.001	15.0 ± 0.1	62.4 ± 0.2
pH 6, 1 M NaCl	-0.136	4.21 ± 0.03	2.15 ± 0.03	2.43E-4 ± 1E-6	0.925 ± 0.001	10.6 ± 0.1	30.7 ± 0.2
pH 9, 1 M NaCl	-0.137	2.48 ± 0.02	0.80 ± 0.01	2.50E-4 ± 1E-6	0.918 ± 0.001	11.8 ± 0.1	36.6 ± 0.2
pH 11, 0.1 M NaCl	-0.197	36.3 ± 0.4	2.7 ± 0.1	2.33E-4 ± 2E-6	0.908 ± 0.001	10.6 ± 0.1	32.9 ± 0.5
pH 12, 0.1 M NaCl	-0.286	29.6 ± 0.2	2.77 ± 0.08	2.16E-4 ± 1E-6	0.934 ± 0.001	12.3 ± 0.1	27.6 ± 0.2
pH 13, 0.1 M NaCl	-0.322	15.8 ± 0.1	2.13 ± 0.04	2.12E-4 ± 1E-6	0.939 ± 0.001	12.1 ± 0.1	26.0 ± 0.2

performed at $f_B = 10$ kHz using cylindrical specimens, since they allow a faster measurement (the higher f_B , the shorter the testing time). The described procedure is an alternative to that proposed by Harrington and Devine.⁴² The capacitance C_B was calculated according to Eq. 2, and C_{SC} was obtained by Eq. 7.

Figure 11 shows the MS plot for a cylindrical specimen after 20 h of polarization at 0.1 V_{SCE} in pH 6, 1 M NaCl at 90°C. A hysteresis was observed between the forward and the reverse scans, indicating that the passive film properties are slightly modified by scanning the potential in the cathodic direction. Each single impedance measurement lasted approximately 7 s, and the total length of the test was 210 s. The same procedure was repeated for different film formation potentials (E_{FF}). The data from the forward scans (cathodic direction) was used for calculating N_D and E_{FB} . Figure 12 shows the MS plots after 20 h of polarization at potentials in the passive range in pH 6, 1 M NaCl at 90°C. Similar results were obtained for the different E_{FF} . The passive film of alloy 22 showed an n-type semiconducting behavior, changing to p-type for the higher potentials. Table III shows the values of N_D and E_{FB} obtained from linear least squares fits of Eq. 1 for each E_{FF} . The obtained parameters did not vary significantly with E_{FF} . The average values were $N_D = 2.7 \times 10^{20}$ cm⁻³ and $E_{FB} = -0.551$ V_{SCE}.

Figure 13 shows the values of C_B as a function of the potential for the EIS tests, and for some of the MS tests in cylindrical specimens of alloy 22 in pH 6, 1 M NaCl at 90°C. The high-frequency and the low-frequency capacitances (C_{B1} and C_{B2}) were plotted for those tests showing two time constants (EIS tests at -0.4, 0.3, and 0.4 V_{SCE}). The capacitance values from MS tests include those after polarizations at -0.2, 0.0 and 0.2 V_{SCE}, in the passive range. The

test performed after polarization at 0.4 V_{SCE}, corresponds to the transpassive film. The capacitance values from the EIS tests correspond to the steady state passive film at each potential. The capacitances of EIS tests were similar to those of MS tests in the full passive range. The capacitances of the MS test of the transpassive film ($E_{FF} = 0.4$ V_{SCE}) were slightly lower than those obtained in the full passive range. These values are shown for comparison, since according to the proposed interpretation the measured capacitance was not that of the film but the interfaces capacitance. The capacitance values were more dependent on the measurement potential than on the passive film formation potential.

Discussion

Electrochemical impedance has been used recently to study passive alloy 22 in chloride solutions.^{14-18,20-27} In some of these studies the data are analyzed in terms of the PDM, while in some other works the interpretation is in terms of electrical analogs. In the present work, equivalent circuits were used for obtaining the ionic and electronic properties of alloy 22. The passive film impedance was found to predominate in the full passive range. The passive film resistance increased and the interfacial capacitance decreased with the polarization time (Fig. 8). The protective properties of the film improved in time under potentiostatic conditions, which may be attributed to film thickening and aging processes. The aging processes include chromium enrichment of the passive film barrier layer and the dehydration of the film.^{3,32} These processes may modify the dielectric constant of the film. The passive film resistance and the thickness of the space charge layer increased with the applied

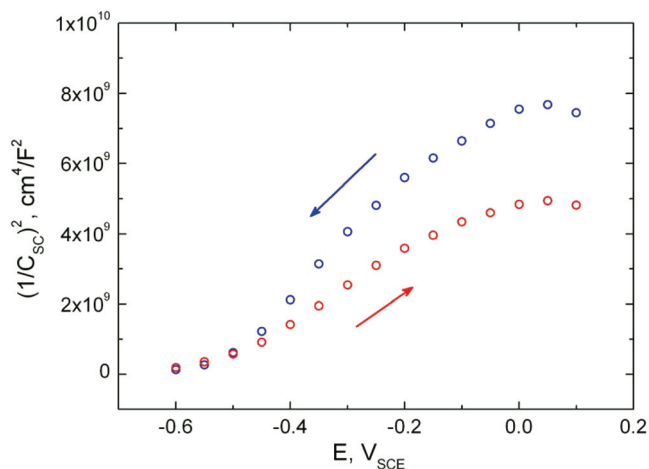


Figure 11. (Color online) MS plot (forward and reverse scans) for a cylindrical specimen after 20 h of polarization at 0.1 V_{SCE} in deaerated pH 6, 1 M NaCl at 90°C. Impedance measured at 10 kHz.

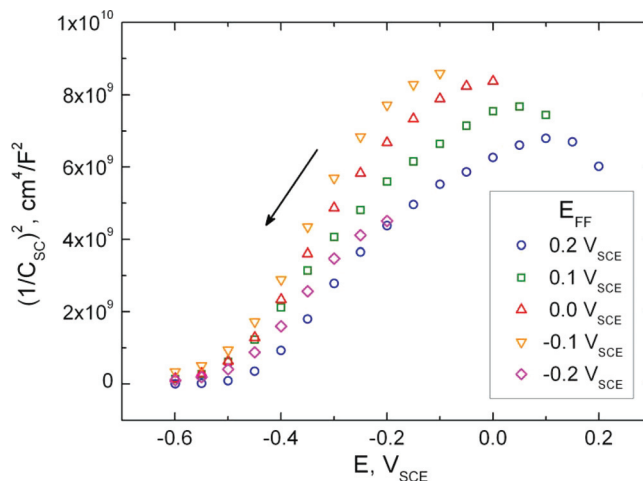


Figure 12. (Color online) MS plot for cylindrical specimens after 20 h of polarization at potentials in the passive range in deaerated pH 6, 1 M NaCl at 90°C. Impedance measured at 10 kHz.

Table III. Parameters obtained from linear least squares fits of the MS equation corresponding to tests in cylindrical specimens of alloy 22 in pH 6, 1 M NaCl at 90°C.

E_{FF} [V _{SCE}]	N_D [cm ⁻³]	E_{FB} [V _{SCE}]	Linear least squares R^2
-0.2	3.20E+20	-0.552	0.988
-0.1	1.97E+20	-0.561	0.995
0.0	2.30E+20	-0.556	0.992
0.1	2.96E+20	-0.570	0.991
0.2	3.18E+20	-0.514	0.989

potential (Fig. 7). The film growth acted to balance the increasing applied potential, and a near-constant electric field was maintained in the film at steady state. The passive film thickness would be that of the space charge layer only if the charge is uniformly distributed across the film. This simple model also applied in open circuit conditions, in a variety of chloride solutions (Figs. 9 and 10). The passive film developed was able to protect the alloy from the environment, even in concentrated and acidic chloride solutions (Table II). The control of the corrosion kinetics was anodic at the open circuit potential, in the studied conditions. The film resistance did not vary significantly with chloride concentration, from 0.1 to 10 M Cl⁻, nor with solution pH, from pH 2 to 13. Near the depassivation pH ($pH_D = 0.3$),¹⁸ the film resistance showed a decrease (Table II). This was correlated with an increase of C_B , indicating the presence of a thinner film. In the most concentrated chloride solution, alloy 22 showed surprisingly the largest film resistance and almost the lowest C_B (thick film). Note that in this solution the cation was changed (Ca²⁺ instead of Na⁺).

The EIS measurements at a low passive potential (-0.4 V_{SCE}) indicated the presence of a second time constant (Fig. 4). However, the fit of the equivalent circuit of Fig. 1c to the experimental data was poor at frequencies below 1 Hz (Fig. 4 and Table I). This indicated that the model does not fully represent the system response in the low frequency domain. Adding a Warburg element to the circuit may improve the goodness of fit, but its physical meaning will not be clear since the temperature was too low for diffusion to be important within the film. This might be a limitation of the equivalent circuit approach and a better interpretation should be sought, which was out of the scope of the present work. The presence of a second time constant was reported previously for alloy 22 and also for chromium.^{16,17,21,31} Gray et al.^{16,17} attribute the low-frequency time constant to the charge transfer at the metal/film and at the film/solution interfaces, while the contribution of the passive film is associated to the high-frequency time constant. Priyantha et al.²¹ applied an

equivalent circuit model consisting in three time constants to the entire passive and transpassive ranges. They do not associate explicitly the processes occurring at the interfaces and in the film to the different time constants or frequency ranges, and the variation of the resistances and capacitances with the applied potential do not show a definite trend. Nevertheless, they report the increase of the total resistance with the applied potential in the passive range, as observed in the present work.²¹ Moffat and Latanision³¹ used the R_{Ω} -CPE circuit model (Fig. 1a) for passive chromium in 1 M H₂SO₄, in the high-frequency range. They associate the low-frequency time constant with reactions of adsorbed protons. Bojinov et al.⁴⁶ suggest the solid state oxidation of Cr²⁺ to Cr³⁺ with a probable partial dehydration, at low passive potentials. In the present work, where two time constant appeared the main resistance to the ion transfer was that of the low frequency one (Table I). The properties of the passive film are usually obtained by measurements in the high frequency range.^{14-18,21} However, for the present experimental conditions, the high frequency resistance was the lowest one, suggesting that for low passive potentials the resistances to the ion transfer would be located at the film interfaces and not within the film.

The potentials 0.3 and 0.4 V_{SCE} were in the range of the transpassive dissolution of alloy 22 (Fig. 2). It was also assumed that the resistances to the ion transfer were located at the film interfaces and not within the film at these potentials. The barrier layer of the passive film of alloy 22 is rich on Cr³⁺ oxide and/or hydroxide.¹³ The solid state oxidation of Cr³⁺ to Cr⁶⁺ proceeded in the film at sufficiently high potentials, and the transpassive dissolution started when the concentration of Cr⁶⁺ in the film reached a critical value.⁴⁶ From the standpoint of the electronic properties of the film, the change from n-type to p-type was observed near 0.0 V_{SCE} (Fig. 12). The transpassive reaction started at a potential where the Fermi level of the metal became lower than the d-band edge of the film.³¹ The cation vacancies are indicated to be the dominant defects of the film in the transpassive state.^{21,22} They are generated at the film/solution interface through the oxidative ejection of cations from the film. The present results indicated a range of potentials in which the alloy showed a p-type electronic behavior, but the ionic transport was slow enough for the film to remain in the passive state. The thickness of space charge layer reached its maximum value approximately at 0.0 V_{SCE}, decreasing for higher potentials (Fig. 7). However, the values of d_{SC} at potentials higher than 0.0 V_{SCE} would not be valid if an inversion layer is formed. The resistance to ion transfer started to decrease from 0.1 to 0.4 V_{SCE}, but its value was large below 0.3 V_{SCE} (Fig. 7). The MS plots showed the change from n-type to p-type character above 0.0 V_{SCE} (Fig. 12), but the polarization curve indicated a sudden current increase only above 0.3 V_{SCE} (Fig. 2). The generation of defects at the film/solution interface was favored by the increase of the potential (driving force). According to the proposed model, the main resistance to the transport of defects was located in the passive film at 0.2 V_{SCE}, but at the film/solution interface at 0.3 and 0.4 V_{SCE}. This resistance decreased or remained constant as the potential increased, giving rise to the observed current increment in Fig. 2.

The effective capacitance of a passive film displaying frequency dispersion may be obtained from different expressions available in the literature. The expressions proposed by Brug et al.⁴⁴ (Eqs. 3 and 5) and by Hsu-Mansfeld⁴⁹ (Eqs. 4 and 6) are commonly used. The former expression is dominated by the ohmic resistance (R_{Ω}) while the latter is dominated by the film resistance (R). Hirschorn et al.⁵⁰ indicate that the expression of Brug et al. holds when the electrode properties vary along the surface (2D) and that of Hsu-Mansfeld holds when the electrode properties vary normal to the surface (3D). According to these authors, the formula of Hsu-Mansfeld should be used for obtaining the effective capacitance of chromium-rich passive films, since they are described as having a resistivity that decays exponentially with position.⁴⁶ As a consequence of this, the capacitance of a passive film behaving as a blocking electrode (Fig. 1a) cannot be calculated since $R \rightarrow \infty$. Harrington and Devine^{25,42} compared the expressions of Brug et al. and

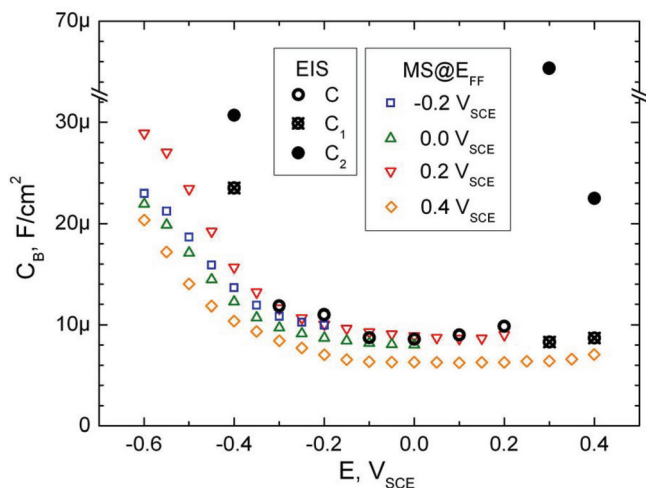


Figure 13. (Color online) Capacitance as a function of the potential for the EIS tests and some of the MS tests in cylindrical specimens of alloy 22 in pH 6, 1 M NaCl at 90°C.

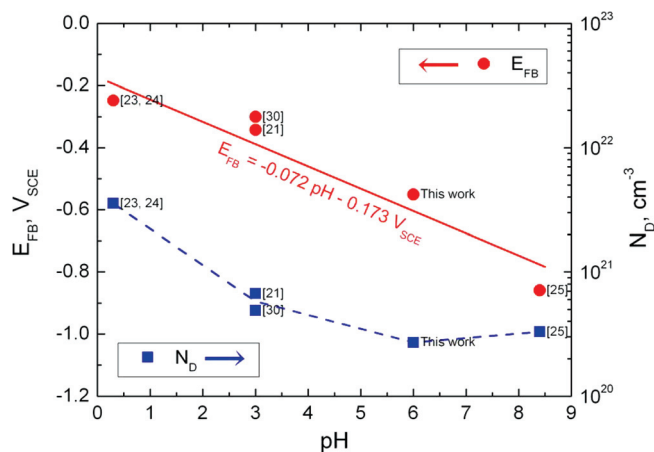


Figure 14. (Color online) Flat band potential and donor density of the passive film of alloy 22 as a function of the solution pH. Results from references (square brackets) and from the present work.

Hsu-Mansfeld for obtaining the flat band potentials and carrier densities of passive nickel, titanium, chromium and alloy 22 *via* the MS analyses. They indicate that the expression of Brug et al. is the most suitable for obtaining the average capacitance. Rodríguez et al.¹⁸ report that the capacitances of passive alloy 22 in acidic chloride solutions obtained from the expression of Hsu-Mansfeld were too large to be associated with a chromium-rich passive film. The same was observed in the present work (Fig. 6 and Table II). The formula of Brug et al. led to capacitance values consistent with the presence of a chromium-rich passive film. The expression of Hsu-Mansfeld led to capacitance values higher than that of the Helmholtz layer.

The capacitance values were more dependent on the measurement potential than on the passive film formation potential (Fig. 13). The interfacial capacitance increased below -0.3 V_{SCE}, indicating the accumulation of charges at the interface, independently of the film formation potential. The same was observed for the transpassive film ($E_{FF} = 0.4$ V_{SCE} in Fig. 13). This accumulation of charges may be due to the solid state reaction $\text{Cr}^{3+} + e^- \leftrightarrow \text{Cr}^{2+}$. Hydrogen adsorption may take place at lower potentials, leading to surface charging.

The passive film of alloy 22 was found to be an n-type semiconductor, which changed to p-type for high passive potentials. The change in the semiconducting character was observed for potentials below those associated with the transpassive dissolution, as discussed above. Average values of $N_D = 2.7 \times 10^{20} \text{ cm}^{-3}$ and $E_{FB} = -0.551$ V_{SCE} were determined in the present work for passive alloy 22 in pH 6, 1 M NaCl. E_{FB} was in agreement with the potential at which the cathodic current of the hydrogen reduction was observed (Fig. 2), as reported elsewhere.²⁵ Figure 14 shows the values of E_{FB} and N_D for alloy 22 from the literature^{21,23–25,30} and from the present work, as a function of the solution pH. The reviewed results include measurements in chloride, sulfate and borate solutions at temperatures from 20 to 90°C. E_{FB} showed the expected Nernst dependence with pH. The obtained slope from linear least squares fit was -0.072 V/pH, which was in agreement with the expected value for the broad temperature range studied. Below pH 3, N_D increased significantly for decreasing pH values. It may be related with a more defective passive film. The influence of pH on E_{FB} and N_D was more important than the effects of the temperature and the anion species.

Summary and Conclusions

The impedance response of passive alloy 22 in chloride solutions at 90°C was analyzed in terms of electrical analogs. EIS tests were performed after long polarization in the passive range and at the onset of the transpassive range, in pH 6 1 M NaCl. A single time constant was observed in the full passive range. The system was

modeled by a R_{Ω} -(R//CPE) equivalent circuit, where R was the film resistance and the CPE dealt with the frequency dispersion of the electrode properties. This simple model applied for a wide range of chloride concentrations (from 0.1 to 10 M Cl⁻) and pH values (from pH 2 to 13), at the open circuit potential. Two time constants were observed at the low passive potential and in the transpassive range. In these cases, the resistances for the ion transfer might be located at the film interfaces and not in the film itself.

The protective properties of the film improved with the polarization time, which was attributed to the thickening and aging of the film. These processes include chromium enrichment and dehydration of the passive film. The film resistance and the space charge layer thickness increased with the applied potential. The oxidation of Cr^{3+} to Cr^{6+} occurred in the film at high potentials, and the transpassive dissolution started when the Cr^{6+} reached a critical concentration. There was a range of potentials in which the film showed a p-type electronic behavior (suggesting the onset of transpassivity), but the ionic transport was slow enough for the film to remain passive under these conditions. This may be explained by considering that the potential is the driving force of the transpassive dissolution. As the potential increases the resistances decrease or remain constant.

The passive film of alloy 22 was an n-type semiconductor, which changed to a p-type for the high passive potentials. Average values of $N_D = 2.7 \times 10^{20} \text{ cm}^{-3}$ and $E_{FB} = -0.551$ V_{SCE} were determined for the n-type semiconductor in pH 6, 1 M NaCl. Comparison of the capacitances obtained from EIS and MS tests indicated that they were more dependent on the measurement potential than on the passive film formation potential.

Acknowledgments

R. M. C. acknowledges financial support from the Agencia Nacional de Promoción Científica y Tecnológica of the Ministerio de Educación, Ciencia y Tecnología from Argentina and from the Universidad Nacional de San Martín.

Appendix

The evaluation of the R_{Ω} -C_B circuit impedance at the characteristic frequency $f_B = \frac{1}{2\pi R_{\Omega} C_B}$ leads to Eq. A-1

$$Z = R_{\Omega} - jR_{\Omega} \quad \text{[A-1]}$$

The R_{Ω} -(R//CPE) circuit can be simplified to a R_{Ω} -CPE circuit in the high-frequency range, since $R \gg R_{\Omega}$. Evaluation of the R_{Ω} -CPE circuit impedance at f_B leads to Eq. A-2

$$Z = R_{\Omega} + \frac{1}{Q} \left(\frac{C_B R_{\Omega}}{j} \right)^{\alpha} = R_{\Omega} + \frac{(R_{\Omega} C)^{\alpha}}{Q} \cdot \cos\left(\frac{-\pi\alpha}{2}\right) + j \frac{(R_{\Omega} C)^{\alpha}}{Q} \cdot \sin\left(\frac{-\pi\alpha}{2}\right) \quad \text{[A-2]}$$

At f_B , the imaginary part of the impedances of the R_{Ω} -C and R_{Ω} -CPE circuits are approximately equal, for $\alpha \rightarrow 1$. It leads to Eq. A-3

$$C_B = \left[\frac{-Q}{\sin\left(\frac{-\pi\alpha}{2}\right)} \right]^{1/\alpha} R_{\Omega}^{\frac{(1-\alpha)}{\alpha}} \quad \text{[A-3]}$$

Since $\lim_{\alpha \rightarrow 1} \sin\left(\frac{-\pi\alpha}{2}\right) = -1$, Eq. A-3 becomes Eq. A-4, which is the expression proposed by Brug et al.,⁴⁴ considering $R \gg R_{\Omega}$

$$C_B = Q^{1/\alpha} R_{\Omega}^{\frac{(1-\alpha)}{\alpha}} \quad \text{[A-4]}$$

References

1. R. B. Rebak, *Corrosion and Environmental Degradation*, Vol. 2, Wiley-VCH, Weinheim, Germany (2000).
2. A. J. Sedriks, *Corrosion of Stainless Steels*, 2nd ed., John Wiley & Sons, New York (1996).
3. P. Marcus and V. Maurice, *Corrosion and Environmental Degradation*, Vol. 2, Wiley-VCH, Weinheim, Germany (2000).
4. N. Sato, *Corros. Sci.*, **31**, 1, (1990).
5. J. W. Schultze and M. M. Lohrengel, *Electrochim. Acta*, **45**, 2499, (2000).

6. D. D. Macdonald, *Pure Appl. Chem.*, **71**, 951 (1999).
7. N. E. Hakiki, S. Boudin, B. Rondot, and M. Da Cunha Belo, *Corros. Sci.*, **37**, 1809 (1995).
8. K. Fujimoto and H. Tsuchiya, *Corros. Sci.*, **49**, 195 (2007).
9. M. F. Montemor, M. G. S. Ferreira, N. E. Hakiki, and M. Da Cunha Belo, *Corros. Sci.*, **42**, 1635 (2000).
10. M. F. Montemor, M. G. S. Ferreira, M. Walls, B. Rondot, and M. Da Cunha Belo, *Corrosion*, **59**, 11 (2003).
11. M. Da Cunha Belo, N. E. Hakiki, and M. G. S. Ferreira, *Electrochim. Acta*, **44**, 2473, (1999).
12. A. C. Lloyd, D. W. Shoesmith, N. S. MacIntyre, and J. J. Noël, *J. Electrochem. Soc.*, **150**, B120 (2003).
13. A. C. Lloyd, J. J. Noël, N. S. MacIntyre, and D. W. Shoesmith, *Electrochim. Acta*, **49**, 3015 (2004).
14. J. J. Gray, J. R. Hayes, G. E. Gdowski, B. E. Viani, and C. A. Orme, *J. Electrochem. Soc.*, **153**, B61 (2006).
15. J. J. Gray, J. R. Hayes, G. E. Gdowski, and C. A. Orme, *J. Electrochem. Soc.*, **153**, B156 (2006).
16. J. J. Gray and C. A. Orme, *Electrochim. Acta*, **52**, 2370 (2007).
17. J. J. Gray, B. S. El Dasher, and C. A. Orme, *Surf. Sci.*, **600**, 2488 (2006).
18. M. A. Rodríguez, R. M. Carranza, and R. B. Rebak, *J. Electrochem. Soc.*, **157**, C1 (2010).
19. G. M. Gordon, *Corrosion*, **58**, 811 (2002).
20. D. D. Macdonald, A. Sun, N. Priyantha, and P. Jayaweera, *J. Electroanal. Chem.*, **572**, 421 (2004).
21. N. Priyantha, P. Jayaweera, D. D. Macdonald, and A. Sun, *J. Electroanal. Chem.*, **572**, 409 (2004).
22. D. D. Macdonald and A. Sun, *Electrochim. Acta*, **51**, 1767 (2006).
23. K. S. Raja, S. A. Namjoshi, and M. Misra, *Mater. Lett.*, **59**, 570 (2005).
24. K. S. Raja and D. A. Jones, *Corros. Sci.*, **48**, 1623 (2006).
25. S. P. Harrington and T. M. Devine, *J. Electrochem. Soc.*, **156**, C154 (2009).
26. M. A. Rodríguez, R. M. Carranza, and R. B. Rebak, *Metall. Mater. Trans. A*, **36A**, 1179 (2005).
27. M. A. Rodríguez, R. B. Rebak, and R. M. Carranza, *Materials Research Society Symposium Proceedings*, Vol. 985, MRS, p. 287 (2007).
28. E. Barsoukov and J. R. Macdonald, *Impedance Spectroscopy: Theory, Experiment, and Applications*, 2nd ed., John Wiley & Sons, Hoboken, NJ (2005).
29. D. D. Macdonald, *J. Electrochem. Soc.*, **139**, 3434 (1992).
30. G. Bellanger and J. J. Rameau, *J. Mater. Sci.*, **31**, 2097 (1996).
31. T. P. Moffat and R. M. Latanision, *J. Electrochem. Soc.*, **139**, 1869 (1992).
32. G. Okamoto, *Corros. Sci.*, **13**, 489 (1973).
33. S. R. Morrison, *Electrochemistry at Semiconductor and Oxidized Metal Electrodes*, 2nd ed., Plenum, New York, NY (1984).
34. D.-S. Kong, S.-H. Chen, C. Wang, and W. Yang, *Corros. Sci.*, **45**, 747 (2003).
35. J. Kim, E. Cho, and H. Kwon, *Electrochim. Acta*, **47**, 415 (2001).
36. H. Tsuchiya, S. Fujimoto, O. Chihara, and T. Shibata, *Electrochim. Acta*, **47**, 4357 (2002).
37. A. Di Paola, *Electrochim. Acta*, **34**, 203 (1989).
38. J. B. Jorcin, M. E. Orazem, N. Pébère, and B. Tribollet, *Electrochim. Acta*, **51**, 1473 (2006).
39. V. M.-W. Huang, V. Vivier, M. E. Orazem, N. Pébère, and B. Tribollet, *J. Electrochem. Soc.*, **154**, C81 (2007).
40. V. M.-W. Huang, V. Vivier, I. Frateur, M. E. Orazem, and B. Tribollet, *J. Electrochem. Soc.*, **154**, C89 (2007).
41. V. M.-W. Huang, V. Vivier, M. E. Orazem, N. Pébère, and B. Tribollet, *J. Electrochem. Soc.*, **154**, C99 (2007).
42. S. P. Harrington and T. M. Devine, *J. Electrochem. Soc.*, **155**, C381 (2008).
43. K. Darowicki, S. Krakowiak, and P. Slepski, *Electrochim. Acta*, **51**, 2204 (2006).
44. G. J. Brug, A. L. G. Van Den Eeden, M. Sluyters-Rehbach, and J. H. Sluyters, *J. Electroanal. Chem.*, **176**, 275 (1984).
45. C. Sunseri, S. Piazza, and F. Di Quarto, *J. Electrochem. Soc.*, **137**, 2411 (1990).
46. M. Bojinov, G. Fabricius, T. Laitinen, T. Saario, and G. Sundholm, *Electrochim. Acta*, **44**, 247 (1998).
47. ASTM International, *Annual Book of ASTM Standards: Wear and Erosion; Metal Corrosion*, Vol. 03.02, ASTM International, West Conshohocken, PA (2005).
48. D. D. Macdonald, A. C. Scott, and P. Wentrczek, *J. Electrochem. Soc.*, **126**, 908 (1979).
49. C. H. Hsu and F. Mansfeld, *Corrosion*, **57**, 747 (2001).
50. B. Hirschorn, M. E. Orazem, B. Tribollet, V. Vivier, I. Frateur, and M. Musiani, *Electrochim. Acta*, **55**, 6218 (2010).